

# <sup>31</sup>P NMR investigation of quasi-two-dimensional magnetic correlations in $T_2P_2S_6$ ( $T = \text{Mn} \& \text{Ni}$ )

F. Bougamha,<sup>1,2</sup> S. Selter,<sup>2</sup> Y. Shemerliuk,<sup>2</sup> S. Aswartham,<sup>2</sup> A. Benali,<sup>1,\*</sup> B. Büchner,<sup>2,3</sup> H.-J. Grafe,<sup>2</sup> and A. P. Dioguardi<sup>2,†</sup>

<sup>1</sup>*Department of Physics, Faculty of Sciences, University of Tunis El-Manar, Tunis 2092, Tunisia*

<sup>2</sup>*Institute for Solid State Research, Leibniz IFW Dresden, Helmholtzstr. 20, 01069 Dresden, Germany*

<sup>3</sup>*Institute of Solid State and Materials Physics and Würzburg-Dresden Cluster of Excellence ct.qmat, Technische Universität Dresden, 01062 Dresden, Germany*

(Dated: December 7, 2021)

We report the anomalous breakdown in the scaling of the microscopic magnetic susceptibility—as measured via the <sup>31</sup>P nuclear magnetic resonance (NMR) shift  $K$ —with the bulk magnetic susceptibility  $\chi$  in the paramagnetic state of  $\text{Mn}_2\text{P}_2\text{S}_6$ . This anomaly occurs near  $T_{\text{max}} \sim 117$  K the maximum in  $\chi(T)$  and is therefore associated with the onset of quasi-two-dimensional (quasi-2D) magnetic correlations. The spin-lattice relaxation rate divided by temperature  $(T_1T)^{-1}$  in  $\text{Mn}_2\text{P}_2\text{S}_6$  exhibits broad peak-like behavior as a function of temperature, qualitatively following  $\chi$ , but displaying no evidence of critical slowing down above the Néel temperature  $T_N$ . In the magnetic state of  $\text{Mn}_2\text{P}_2\text{S}_6$ , NMR spectra provide good evidence for 60 degree rotation of stacking-fault-induced magnetic domains, as well as observation of the spin-flop transition that onsets at 4 T. The temperature-dependent critical behavior of the internal hyperfine field at the P site in  $\text{Mn}_2\text{P}_2\text{S}_6$  is consistent with previous measurements and the two-dimensional anisotropic Heisenberg model. In a sample of  $\text{Ni}_2\text{P}_2\text{S}_6$ , we observe only two magnetically split resonances in the magnetic state, demonstrating that the multiple-peaked NMR spectra previously associated with 60 degree rotation of stacking faults is sample dependent. Finally, we report the observation of a spin-flop-induced splitting of the NMR spectra in  $\text{Ni}_2\text{P}_2\text{S}_6$ , with an onset spin-flop field of  $H_{\text{sf}} = 14$  T.

## I. INTRODUCTION

The  $T_2P_2Ch_6$  family [1] of quasi-two-dimensional (quasi-2D) magnetic van der Waals (vdWs) materials ( $T = \text{Mn}, \text{Ni}, \text{Fe}, \text{Co}$ ; and  $Ch = \text{S}, \text{Se}$ ) are currently the subject of broad and intense attention as a model system of low-dimensional magnetism, transport, and novel devices for technological applications in valleytronics [2] and spintronics [3]. These magnetic vdWs materials have attracted significant interest, not only because of their technological significance, but also because they allow investigation of fundamental questions related to magnetism in low-dimensional systems [4].

The  $T_2P_2S_6$  subfamily (with  $T = \text{V}, \text{Mn}, \text{Fe}, \text{Co}, \text{Ni}$ ) has been investigated due to a variety of interesting physical and chemical properties, such as with regards to anisotropy [5–8], their potential applications as cathode materials for secondary batteries [9], ferroelectric properties [10], optically active nonlinear properties [11–13] and ion-exchange applications [14]. Moreover, the ability of these quasi-2D vdWs materials to accommodate extrinsic intercalated species in the vdWs gap leads to a drastic change of their magnetic, electrical, and optical properties [9].

The first synthesis of a  $T_2P_2S_6$  compound was reported by M. C. Friedel *et al.* in 1894 [5, 15]. But, only in the 1970's, were more detailed structural stud-

ies carried out [16–18]. Recently, it has been discovered that  $\text{Mn}_2\text{P}_2\text{S}_6$  and  $\text{Ni}_2\text{P}_2\text{S}_6$  compounds are excellent platforms for investigating correlated electrons in 2D magnetic materials [19–21]. Theoretical and experimental high-pressure research revealed the existence of insulator-to-metal transitions in  $\text{Mn}_2\text{P}_2\text{S}_6$  [20, 22] and  $\text{Ni}_2\text{P}_2\text{S}_6$  [20, 23]. From a quasi-2D magnetic standpoint,  $\text{Mn}_2\text{P}_2\text{S}_6$  has been studied in the antiferromagnetic (AFM) 2D anisotropic Heisenberg model on a honeycomb lattice [7]. Whereas, theoretical investigations reveal that the magnetic anisotropy of  $\text{Ni}_2\text{P}_2\text{S}_6$  is well treated by the XXZ model or a weakly anisotropic Heisenberg model [14, 24, 25].

At ambient pressure,  $\text{Mn}_2\text{P}_2\text{S}_6$  is a highly resistive broad band semiconductor with a gap close to 3 eV and is optically transparent and green in color [26].  $\text{Mn}_2\text{P}_2\text{S}_6$  crystallizes in the monoclinic space group  $C2/m$ , with the Mn sites forming a honeycomb-like structure in the layer planes. The ambient temperature and pressure lattice parameters are  $a = 6.05(1)$  Å,  $b = 10.52(3)$  Å,  $c = 6.80(2)$  Å,  $\alpha = 90^\circ$   $\beta = 107.3(2)^\circ$ , and  $\gamma = 90^\circ$  [27].

Fig. 1(a) shows local environment of the P dimers in the crystal structure. The weak interlayer coupling mediated by the S atoms, was proposed to be purely of vdWs origin. The study of the transition from the paramagnetic state to the antiferromagnetic state collinear phase at 78 K, on the other hand, indicates an interplane exchange related with some degree of metal-ligand covalency [28, 29]. Neutron powder diffraction reveals a transition to the AFM state at 78 K with the Mn moment of  $4.43 \pm 0.03 \mu_B$  canted  $\sim 8^\circ$  from  $c^*$  toward the  $a$  direction [27], indicated by black vectors in Fig. 1(a).

\* ali.benali@fst.utm.tn

† adioguardi@gmail.com

$^{31}\text{P}$  nuclear magnetic resonance (NMR) studies were previously carried out on several  $T_2\text{P}_2\text{S}_6$  [18, 30, 31], and revealed that NMR is a sensitive probe of magnetism. However, these studies were carried out on samples that showed significant magnetic field dependence of the Néel temperature  $T_N$ .

Several recent studies have investigated the transition-metal-substitution dependence of the bulk magnetic properties of these compounds, revealing excellent tunability of the quasi-2D magnetic behavior in  $T_2\text{P}_2\text{S}_6$  compounds [32–34]. This tunability motivates comparison of our recent  $^{31}\text{P}$  nuclear magnetic resonance (NMR) study of  $\text{Ni}_2\text{P}_2\text{S}_6$  [35] to  $\text{Mn}_2\text{P}_2\text{S}_6$ . Theoretical investigations should be focused on the relationship between the magnetic order and anisotropy in detail to the already experimentally investigated systems, such as  $(\text{Mn}_{1-x}\text{Ni}_x)_2\text{P}_2\text{S}_6$  and  $(\text{Mn}_{1-x}\text{Fe}_x)_2\text{P}_2\text{S}_6$  [33, 36]. An important piece of the puzzle is the so-called  $K$ - $\chi$  anomaly in  $\text{Ni}_2\text{P}_2\text{S}_6$ , which occurs in proximity to  $T_{\text{max}} \sim 262\text{ K}$  the maximum in the magnetic susceptibility, and indicates that the microscopic susceptibility observed via NMR provides unique local information about magnetic correlations. Systematic comparison of the interplay between magnetic anisotropy, magnetic interactions, and the  $K$ - $\chi$  anomaly in the quasi-2D magnets Ni and Mn end member compounds may help to shed light on the nature of the quasi-2d correlations in these systems.

In this work we investigate high-quality  $\text{Mn}_2\text{P}_2\text{S}_6$  and  $\text{Ni}_2\text{P}_2\text{S}_6$  single crystals that allow for sensitive  $^{31}\text{P}$  NMR measurements. We find that  $\text{Mn}_2\text{P}_2\text{S}_6$  also exhibits a  $K$ - $\chi$  anomaly, thus strengthening the conclusion that the anomaly is driven by quasi-2D magnetic correlations that emerge near the peak in the magnetic susceptibility ( $T_{\text{max}} \sim 117\text{ K}$ ) but above  $T_N$ . Furthermore, we observe effects of the quasi-2D magnetic fluctuations in  $\text{Mn}_2\text{P}_2\text{S}_6$  via the nuclear spin–lattice relaxation rate divided by temperature  $(T_1T)^{-1}$ .  $(T_1T)^{-1}$  in qualitatively follows  $\chi$ , the peak-like shape of which is associated with quasi-two-dimensional magnetic correlations, indicating that  $(T_1T)^{-1}$  is a good measure of quasi-2D fluctuations. However, similar in the case of  $\text{Ni}_2\text{P}_2\text{S}_6$ , we do not observe any indication of critical slowing down above  $T_N$ . We also find that, in one of two measured crystals of  $\text{Ni}_2\text{P}_2\text{S}_6$ , there exist only two magnetically split peaks for all sample orientations. This indicates that the multiple-peaked NMR spectrum in the magnetic state—thought to be associated with 60 degree rotation of stacking faults—is sample dependent. Finally, we report the observation of a spin-flop transition in  $\text{Ni}_2\text{P}_2\text{S}_6$  at  $H_{\text{sf}} = 14\text{ T}$ .

## II. CRYSTAL SYNTHESIS AND EXPERIMENTAL DETAILS

Two crystals of  $\text{Mn}_2\text{P}_2\text{S}_6$  were measured via NMR (hereafter referred to as  $\text{Mn}_2\text{P}_2\text{S}_6$  crystals A and B). The crystals were plate-like, transparent and green in color,

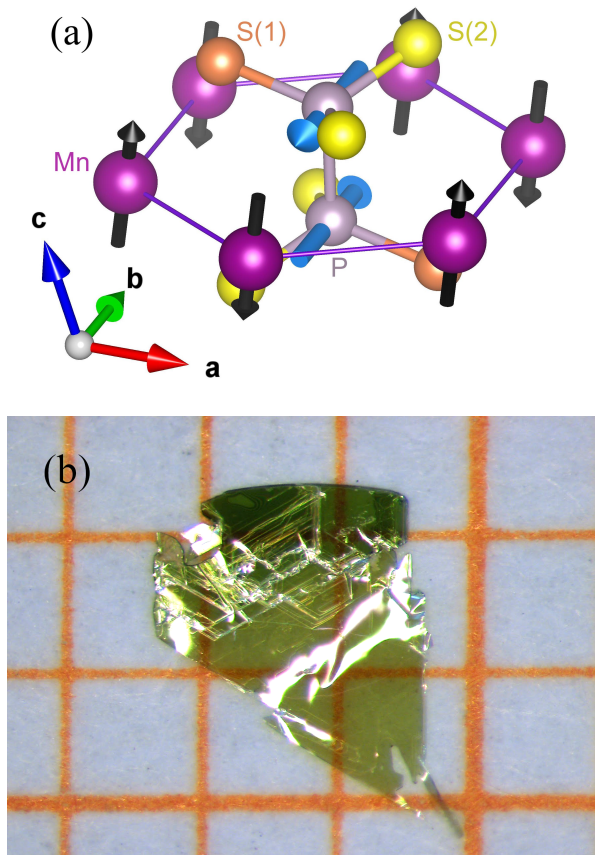


FIG. 1. (a) Local environment of the magnetically inequivalent P sites in  $\text{Mn}_2\text{P}_2\text{S}_6$  [37]. Mn are shown in purple, S(1) in orange, S(2) in yellow, and P in pale pink. Black vectors represent the magnetic moments on the Mn sites [27], and blue vectors represent the calculated dipolar hyperfine field at the P sites due to the Mn magnetic moments [38]. (b) Optical microscope image of  $\text{Mn}_2\text{P}_2\text{S}_6$  crystal B on a mm grid.

and on the order of 1 mg (see Fig. 1(b)). One crystal of  $\text{Ni}_2\text{P}_2\text{S}_6$  was remeasured in this work, and was previously described in Ref. [35]; we refer to this sample as  $\text{Ni}_2\text{P}_2\text{S}_6$  crystal A, the same designation as the previous report. Details of the crystal growth via vapor transport and characterization can be found elsewhere [32, 33, 35]. NMR was measured on the  $^{31}\text{P}$  nuclei (spin  $I = 1/2$ , natural abundance 100%, and gyromagnetic ratio  $^{31}\gamma/2\pi = 17.25144\text{ MHz/T}$  [39]). All raw NMR shift values were calculated with respect to a  $^{31}\text{P}$  standard sample of 85%  $\text{H}_3\text{PO}_4$  in water ( $f_0 = 121.544 \pm 0.001\text{ MHz}$ ).  $^{33}\text{S}$  and  $^{55}\text{Mn}$  NMR were also attempted, but without success. In the case of  $^{33}\text{S}$  this is likely due to the low natural abundance of the NMR-active isotope. In the case  $^{55}\text{Mn}$ , the large on-site magnetic moment is likely responsible for the lack of observability, which can result in a very large relaxation rate and/or shifts larger than 5%.

We note that  $\text{Mn}_2\text{P}_2\text{S}_6$  crystal A was slightly deformed upon insertion into the NMR coil. This resulted in broadening of the spectra into a double-peak in the paramag-

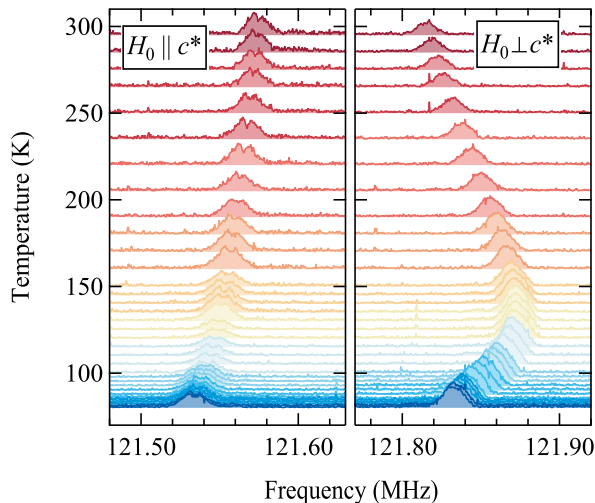


FIG. 2.  $^{31}\text{P}$  NMR frequency spectra as a function of temperature from  $\text{Mn}_2\text{P}_2\text{S}_6$  crystal B for (left)  $H_0 \parallel c^*$  and (right)  $H_0 \perp c^*$  with nominal  $H_0 = 7\text{ T}$ .

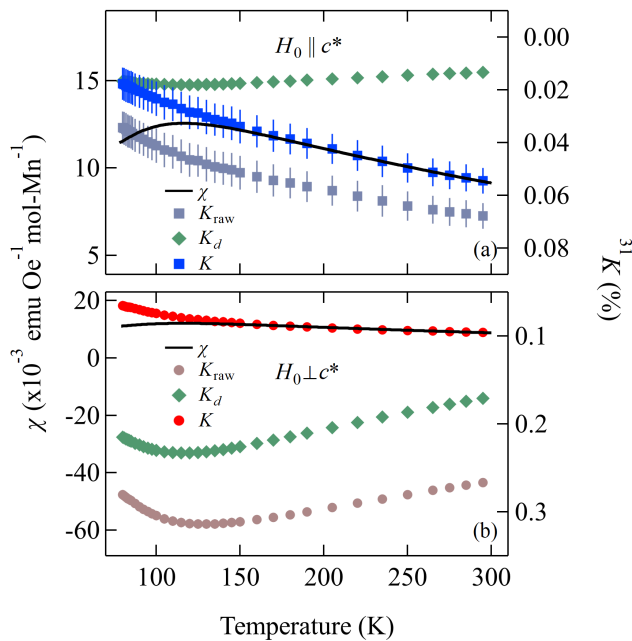


FIG. 3.  $\text{Mn}_2\text{P}_2\text{S}_6$  magnetic susceptibility  $\chi$  (solid lines) and NMR shift  $^{31}K$  (markers) a function of temperature for (a)  $H_0 \parallel c^*$  and (b)  $H_0 \perp c^*$ . The axes have been scaled to highlight the deviation from scaling below approximately 150 K and clearly outside of the experimental uncertainties below  $T_{\text{max}}$ . The raw shift  $K_{\text{raw}}$  was extracted from Gaussian fits to the data in Fig. 2, with respect to the  $^{31}\text{P}$  in 85%  $\text{H}_3\text{PO}_4$  in water. The shift  $K = K_{\text{raw}} - K_d$ , where  $K_d$  is the contribution from bulk magnetic effects as discussed in the text.

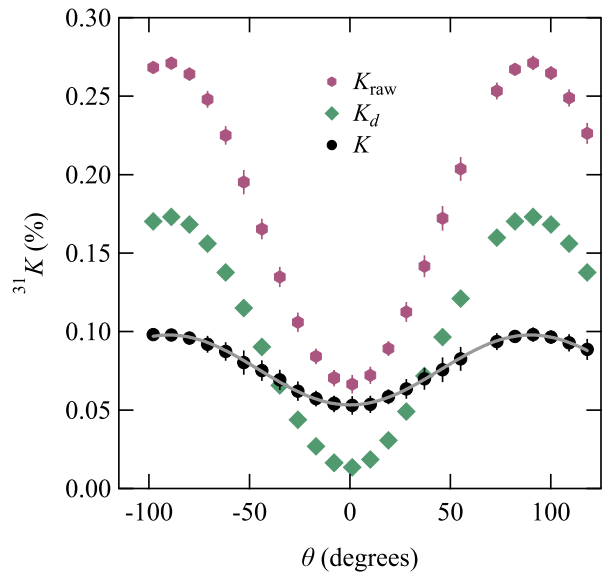


FIG. 4.  $\text{Mn}_2\text{P}_2\text{S}_6$  NMR shift  $^{31}K$  as a function of out-of-plane angle  $\theta$  (black circles), where  $\theta = 0^\circ$  indicates  $H_0 \parallel c^*$ . The grey curve is a fit to Eqn. 1 as described in the text, which yields the fit parameters  $K_{c^*} = 0.053 \pm 0.002\%$  and  $K_{ab} = 0.098 \pm 0.001\%$ . The raw shift  $K_{\text{raw}}$  (salmon hexagons) and the contribution from bulk magnetic effects  $K_d$  (green diamonds) are shown for completeness.

netic state. This double peak was absent in  $\text{Mn}_2\text{P}_2\text{S}_6$  crystal B, which was pristine. While measurements in the magnetic state were unaffected by this physical deformation, the paramagnetic state measurements required a double-peak Gaussian fit to characterize the spectra. Therefore, all normal-state spectral measurements shown in this work were conducted on  $\text{Mn}_2\text{P}_2\text{S}_6$  crystal B. We note however, that double-peak fits to the spectra from  $\text{Mn}_2\text{P}_2\text{S}_6$  crystal A yield identical hyperfine couplings, temperature dependence, and angular dependence.

NMR spectra were collected via standard spin-echo and free-induction-decay (FID) pulse sequences as function of temperature, frequency, and angle. In the magnetic state, when the spectrum becomes too broad to acquire with a single spin echo or FID, we utilize computer-controlled stepper motors to tune and match the resonant circuit and sum the resulting Fourier transforms to reconstruct the intrinsic spectra.

### A. Paramagnetic State Measurements

NMR spectra as a function of temperature are shown in Fig. 2 for both  $H_0 \parallel c^*$  and  $H_0 \perp c^*$ . The raw NMR shifts  $K_{\text{raw}}$  were extracted with respect  $\text{H}_3\text{PO}_4$ , and bulk magnetic effects  $K_d$  were subtracted, assuming an ellipsoidal crystal shape as described previously [35, 40] using the approximate crystal dimensions of  $\text{Mn}_2\text{P}_2\text{S}_6$  crystal B ( $L_x = 2.2\text{ mm}$ ,  $L_y = 1.6\text{ mm}$ , and  $L_z = 0.1\text{ mm}$ ). The resulting NMR shifts  $K$  are shown in Fig. 3 as a function

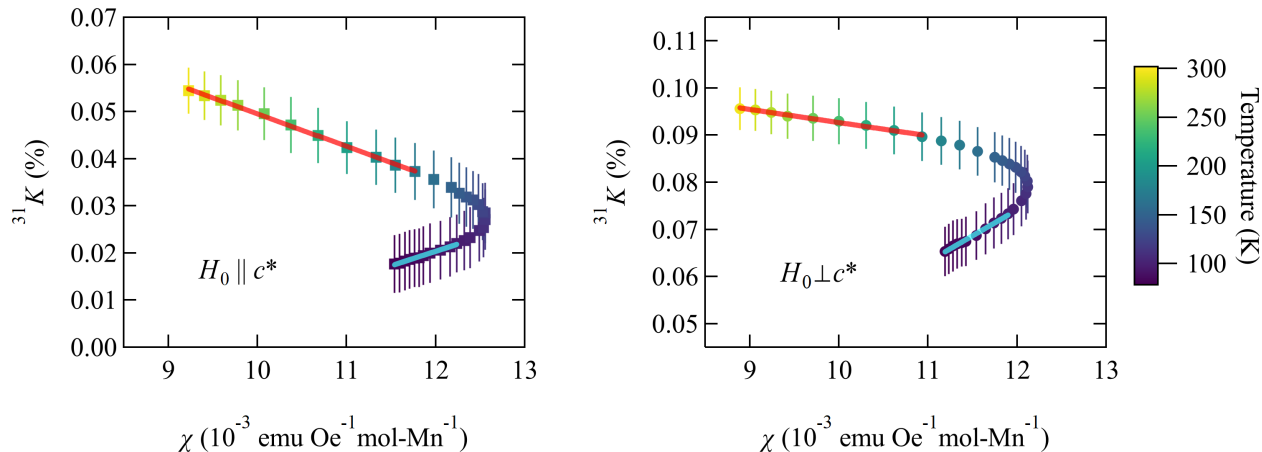


FIG. 5.  $\text{Mn}_2\text{P}_2\text{S}_6$  NMR shift  ${}^{31}\text{K}$  as a function of magnetic susceptibility  $\chi$  with temperature as an implicit parameter. Lines are fits to extract the hyperfine coupling  $A$  and orbital shift  $K_0$  as summarized in Table I.

of temperature along with the bulk magnetic susceptibility (measured in the same applied field of 7 T). The high-temperature data have been scaled to show the striking  $K$ - $\chi$  anomaly that manifests below 150 K.

We also measured the angular dependence of the NMR spectrum at 295 K, and perform the same correction for bulk magnetization effects, with angular dependence of the susceptibility included. The results are shown in Fig. 4. There is no in-plane angular dependence to within the experimental error, therefore, considering also the axial symmetry of the local P environment, we make the assumption that the NMR shift tensor is axially symmetric, i.e.  $K_a = K_b = K_{ab} \neq K_{c^*}$ . The grey curve in Fig. 4 is a least-squares fit to the expected out-of-plane angular dependence

$$K(\theta) = K_{\text{iso}} + K_{\text{ax}} \left( 3 \cos^2 \left[ (\theta - \theta_0) \frac{\pi}{180} \right] - 1 \right), \quad (1)$$

where  $K_{\text{iso}} = \frac{1}{3}(2K_{ab} + K_{c^*})$  and  $K_{\text{ax}} = \frac{1}{3}(K_{c^*} - K_{ab})$ . The resulting best fit is described by the parameters  $K_{c^*} = 0.053 \pm 0.002\%$  and  $K_{ab} = 0.098 \pm 0.001\%$ .

To better highlight the shift anomaly, we also plot  $K$  as a function of  $\chi$  with temperature as an implicit parameter in Fig. 5. One expects  $K \propto \chi$ , and therefore linear relations on such plots (also known as Clogston-Jaccarino plots [41]). The constant—which in the case of an anisotropic material, is actually a tensor quantity—of proportionality in an uncorrelated material is the hyperfine coupling  $\mathbf{A}$ . In the case of  $\text{Mn}_2\text{P}_2\text{S}_6$ , however, we observe two different regions of linear behavior with a change in the sign of the slope in between. The linear fits shown in red and blue in Fig. 5 are characterized by the fit parameters in Table I. The fit ranges are as follows: for  $H_0 \parallel c^*$  the high temperature fit range is  $175 \text{ K} \leq T \leq 285 \text{ K}$  and the low temperature range is  $80 \text{ K} \leq T \leq 93 \text{ K}$ , and for  $H_0 \perp c^*$  the high temperature fit range is  $175 \text{ K} \leq T \leq 295 \text{ K}$  and the low temperature range is  $80 \text{ K} \leq T \leq 102 \text{ K}$ . We note that the low

	High Temperature	Low Temperature
$A_{c^*}$	$-0.04 \pm 0.01 \text{ T}/\mu_B$	$0.03 \pm 0.05 \text{ T}/\mu_B$
$A_{ab}$	$-0.02 \pm 0.01 \text{ T}/\mu_B$	$0.06 \pm 0.04 \text{ T}/\mu_B$
$K_{0,c^*}$	$0.12 \pm 0.02\%$	$-0.1 \pm 0.1\%$
$K_{0,ab}$	$0.12 \pm 0.02\%$	$-0.06 \pm 0.08\%$

TABLE I.  $\text{Mn}_2\text{P}_2\text{S}_6$  hyperfine coupling constants  $A$  and orbital shifts  $K_0$  extracted from fits to  ${}^{31}\text{K}$  vs  $\chi$  as shown in Fig 5.

temperature fits produce a “hyperfine coupling,” but we hesitate to ascribe meaning to this, as will be discussed below.

As mentioned above, we find that the full width at half maximum (FWHM) of the spectra in  $\text{Mn}_2\text{P}_2\text{S}_6$  is significantly larger than in  $\text{Ni}_2\text{P}_2\text{S}_6$  (see Fig. 6). Considering the large magnitude of the bulk magnetic susceptibility, and the FWHM scales qualitatively with the bulk magnetic susceptibility, we conclude that this is the dominant contribution to the increased linewidth.

## B. Antiferromagnetic State Measurements

NMR is an excellent probe of magnetic order; the key measurable parameter is the internal hyperfine field at the P site. We measured the  ${}^{31}\text{P}$  NMR spectra as a function of angle and temperature in the antiferromagnetic state. The angular dependence of the spectra is shown in Fig. 7. We perform multipoint fitting to extract the angular dependence of the resonances. The spectra were collected in an external field of 7 T, which is above the spin-flop field  $T_{\text{sf}} = 4 \text{ T}$ . As a result, the spectra collapse to two split peaks for  $H_0$  nearly parallel to the  $c^*$  direction as the internal hyperfine field is perturbed by the

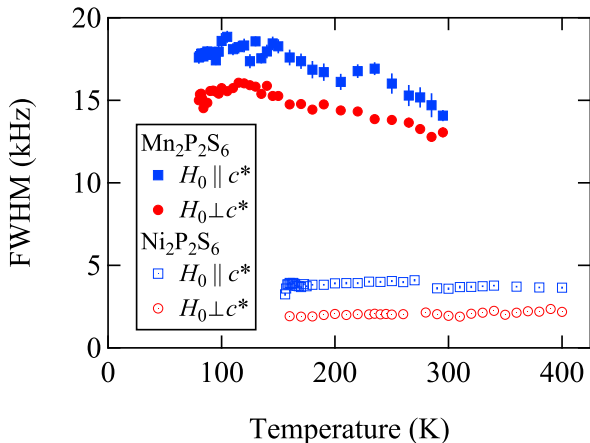


FIG. 6. Full width at half maximum (FWHM) of the  $^{31}\text{P}$  resonances for  $\text{Mn}_2\text{P}_2\text{S}_6$  and  $\text{Ni}_2\text{P}_2\text{S}_6$  as a function of temperature in the paramagnetic state.  $\text{Ni}_2\text{P}_2\text{S}_6$  data are from Ref. [35]  $\text{Mn}_2\text{P}_2\text{S}_6$  data are from single-peak fits to the spectra in Fig. 2.

7 T external field's influence on the Mn moments. The in-plane rotation spectra are not significantly perturbed, as the external field aligned in the basal plane is approximately perpendicular to the easy axis, and therefore does not result in a spin flop. We find six magnetically split peaks, that fall onto a single curve when offset by  $\pm 60^\circ$ . This phenomenon was also observed in the crystal B of  $\text{Ni}_2\text{P}_2\text{S}_6$  [35], and has been associated with stacking faults. We also tracked the internal hyperfine field as a function of temperature in the magnetic state, as shown in Fig. 8.

The internal field allows us to use NMR to carefully measure the spin-flop transition as a function of applied external field. We first aligned the  $\text{Mn}_2\text{P}_2\text{S}_6$  in the normal state such that the applied external field was nearly parallel to  $c^*$ , and then cooled the crystal to 65.3 K. We fit the two resulting magnetically split peaks to a double Gaussian function, holding the amplitudes and widths equal. We extract the component of the internal field along the  $c^*$  direction, which is approximately zero at low fields, but begins to grow starting at  $H_{\text{sf}} = 4$  T and saturates above 7 T. We note that previous measurements find equivalent field dependence associated with a spin-flop transition at low temperatures, indicating that our NMR measurements at higher temperatures in the AFM state are valid [42, 43]. We choose to measure at high temperature due to the extremely slow spin-lattice relaxation rates deep in the AFM state.

We then conducted the same experiment on  $\text{Ni}_2\text{P}_2\text{S}_6$  crystal A, but with  $H_0$  along  $a$ , which remarkably yield a similar result, summarized in Fig. 9. These results provide good evidence for a previously unreported spin-flop transition in  $\text{Ni}_2\text{P}_2\text{S}_6$  with a spin-flop field of  $H_{\text{sf}} = 14$  T. Furthermore, in  $\text{Ni}_2\text{P}_2\text{S}_6$  crystal A, we also discovered that there are only two magnetically split peaks at 5 T

for all in-plane crystal orientations (see Fig. 10), indicating that stacking faults are not present in this crystal. Therefore, we conclude that the presence of stacking faults is sample dependent. The spin-flop transition exists in both  $\text{Mn}_2\text{P}_2\text{S}_6$  and  $\text{Ni}_2\text{P}_2\text{S}_6$  in different field orientations, which is associated with their magnetic moment direction. As shown in the Fig. 1(a) and Fig. 1 in Ref. [35], respectively. The Mn moments in  $\text{Mn}_2\text{P}_2\text{S}_6$  are oriented in a mostly out-of-plane orientation, while the Ni moments in  $\text{Ni}_2\text{P}_2\text{S}_6$  are oriented mostly in the  $a$ -direction, with a small component along the  $c$  direction [44]. In collinear AFM systems, a magnetic field along the easy axis that exceeds a critical spin-flop field  $H_{\text{sf}}$  induces the magnetic moments to rotate [34].

### C. Relaxation Measurements

The spin-lattice relaxation rate was measured for both orientations of  $\text{Mn}_2\text{P}_2\text{S}_6$  crystal A as a function of temperature via saturation recovery, and the data are summarized in Fig. 11. The spin-lattice relaxation rate divided by temperature  $(T_1T)^{-1}$  increases slightly with decreasing temperature down to approximately 150 K, and then decreases, qualitatively following the bulk magnetic susceptibility.

We also measured the spin-spin relaxation by fitting the echo-decay curves, which show a combination of exponential and Gaussian behavior and an oscillatory behavior [45]:

$$M(\tau) = M \exp \left[ -\frac{1}{2} \left( \frac{2\tau}{T_{2g}} \right)^2 \right] \times \left( 1 - F \exp \left[ -\frac{2\tau}{T_2'} \right] \cos [2\tau\omega_{\text{int}} - \psi] \right), \quad (2)$$

where  $\omega_{\text{int}} = ^{31}\gamma H_{\text{int}}$  and  $\psi$  is a phase shift. The fit coefficients are summarized in Fig. 12. Gaussian-like rate component  $T_{2g}$  is temperature independent, while the exponential rate only begins to decrease below approximately 200 K for  $H_0 \parallel c^*$ . The extracted internal field from the oscillatory behavior is temperature independent.

## III. DISCUSSION

The most interesting result in this work is the observation of a shift anomaly in a second member of the  $T_2\text{P}_2\text{S}_6$  family, with the first being  $\text{Ni}_2\text{P}_2\text{S}_6$ . Similar to the Ni case, the Mn sister compound has a shift anomaly that onsets approximately at  $T_{\text{max}}$ , the temperature at which  $\chi$  goes through a maximum. However, in the current case of  $\text{Mn}_2\text{P}_2\text{S}_6$  the shift anomaly also shows a new behavior; not only does the  $K$  fail to scale with  $\chi$ , but the value of the apparent hyperfine coupling changes sign.

NMR shift anomalies have been observed in a few families of materials, including the heavy-fermion compounds

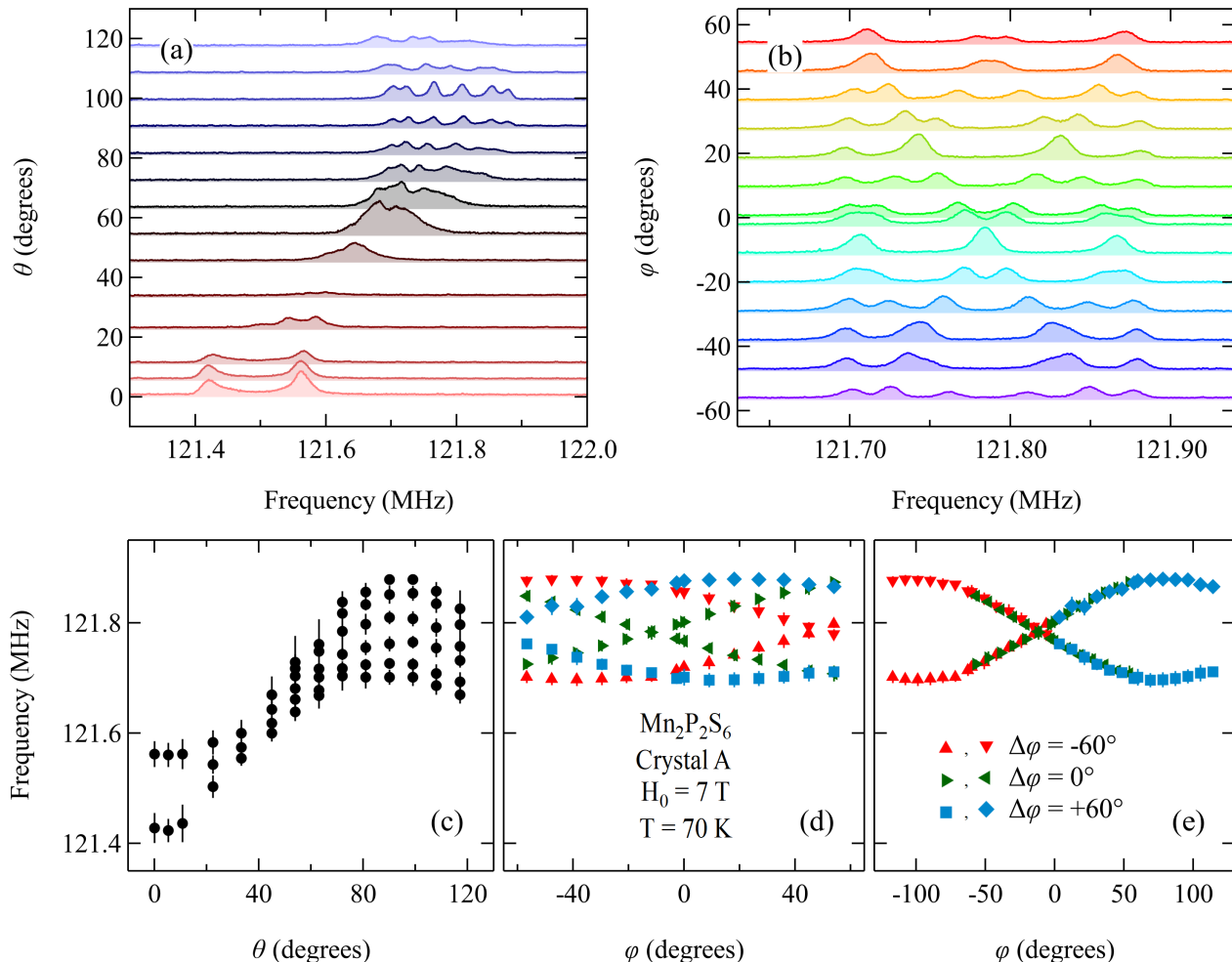


FIG. 7.  $\text{Mn}_2\text{P}_2\text{S}_6$   $^{31}\text{P}$  NMR spectra offset by out-of-plane angle  $\theta$  ( $\theta = 0$  degrees corresponds to  $H_0 \parallel c^*$ ) (a) and in-plane angle  $\varphi$  in the magnetic state at  $T = 70$  K. (c) Frequencies vs  $\theta$  extracted from multi-peak fits to the spectra in (a). (d) Frequencies vs  $\varphi$  extracted from (b) by the same method. (e) In-plane rotation center frequencies from (d) offset by  $-60$ ,  $0$ , and  $60$  degrees. The markers/colors in (d) and (e) were chosen by hand to indicate the unique resonances.

$\text{CeCu}_2\text{Si}_2$ ,  $\text{UPt}_3$ , and  $\text{URu}_2\text{Si}_2$  [46, 47], cuprates [48–50], and most recently iron-based superconductors  $X\text{Fe}_2\text{As}_2$  ( $X = \text{K}, \text{Rb}, \text{Cs}$ ) [51]. NMR offers a unique window into the emergence of electronic correlations via the NMR shift [47]. More interestingly, the NMR shift anomaly has been observed to obey a universal scaling in a particular temperature regime across a dozen heavy-fermion materials, which has attracted considerable attention among various exotic behaviors of heavy-electron materials [52].

In  $\text{Ni}_2\text{P}_2\text{S}_6$  and  $\text{Mn}_2\text{P}_2\text{S}_6$  there exist no conduction electrons, no structural transition is present that could conceivably modify the hyperfine coupling, and the lowest energy crystal field transition from the ground state  $^6A_{1g}$  to the first excited state  $^4T_{1g}$  is 1.92 eV [53]. Therefore, another effect must be responsible for the  $K$ - $\chi$  anomaly. Considering the proximity to  $T_{\text{max}}$  in both materials, which in turn is a phenomenon associated with quasi-2D magnetic fluctuations, we take the observation

of a shift anomaly in  $\text{Mn}_2\text{P}_2\text{S}_6$  as further evidence in favor of this conclusion. Two other studies also find a link between quasi-2D magnetic fluctuations and an NMR shift anomaly [54, 55]. Additionally, neutron scattering directly evidences short-range magnetic order for  $T > T_N$  in the related  $\text{Mn}_2\text{P}_2\text{Se}_6$  [56].

Although we do not see any appreciable line broadening or loss of spectral weight near  $T_{\text{max}}$ , it is conceivable that slow fluctuations sample off-diagonal elements of the hyperfine coupling tensor. Note that there is loss of spectral weight starting at about 85 K in  $\text{Mn}_2\text{P}_2\text{S}_6$ , likely due to slight broadening of the magnetic transition, though this is well below  $T_{\text{max}} \sim 117$  K. Therefore, we calculated the dipole-dipole hyperfine coupling tensor of the  $^{31}\text{P}$  nuclei to the Mn magnetic moments via a lattice sum method [57]. These calculations were carried out by building a lattice of Mn spin sites within 600 Å radius of the  $^{31}\text{P}$  probe positions based on the lattice param-

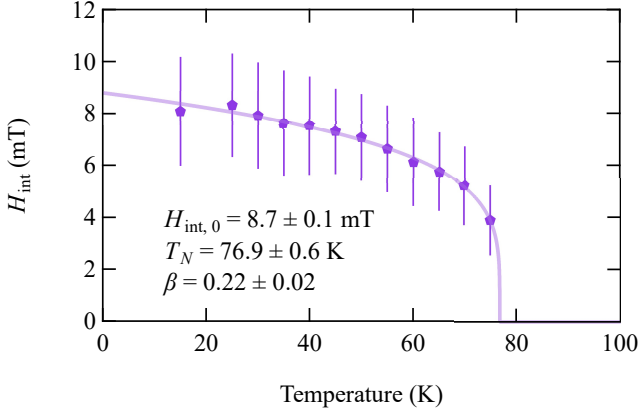


FIG. 8. Temperature dependence of the internal field  $H_{\text{int}}$  obtained from NMR spectra of  $\text{Mn}_2\text{P}_2\text{S}_6$  measured for  $H_0 \perp c^*$  in the magnetic state. The light purple line is the fit to Equation 5 as described in the text. Error bars indicate  $\sigma$  of the distribution of internal fields, uncertainties of peak value of  $H_{\text{int}}$  are smaller than the marker size.

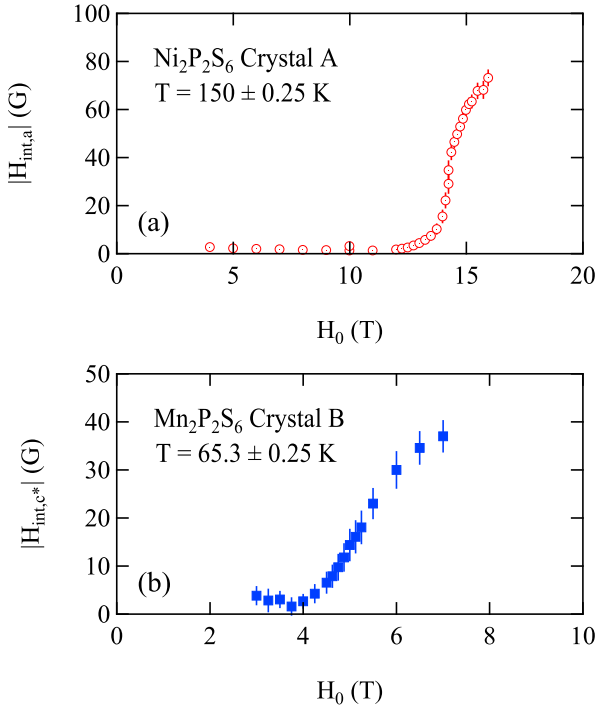


FIG. 9. Component of the internal field parallel to the applied external field as a function of  $H_0$ , showing evidence of the spin-flop transition, which begins at (a) 14 T in the case of  $\text{Ni}_2\text{P}_2\text{S}_6$  with  $H_0$  aligned approximately along  $a$  and (b) 4 T in the case of  $\text{Mn}_2\text{P}_2\text{S}_6$  for  $H_0$  aligned along approximately with  $c^*$ .

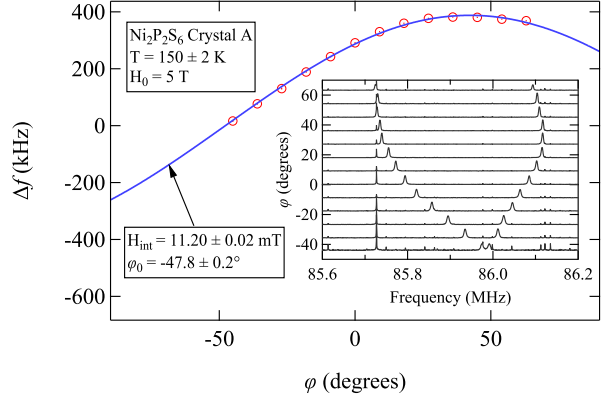


FIG. 10. In-plane angular dependence of the  $^{31}\text{P}$  magnetic peak splitting  $\Delta f$  as a function of in-plane angle  $\varphi$  for  $\text{Ni}_2\text{P}_2\text{S}_6$  crystal A at  $T = 150 \pm 2$  K and  $H_0 = 5$  T. The inset shows the raw frequency-swept spectra. Note that the magnet was in persistent mode for these measurements, and the field likely drifted enough to shift the spectra from one measurement to the next. This has no effect on the splitting.  $H_{\text{int}} = 10.5$  mT for sample B.

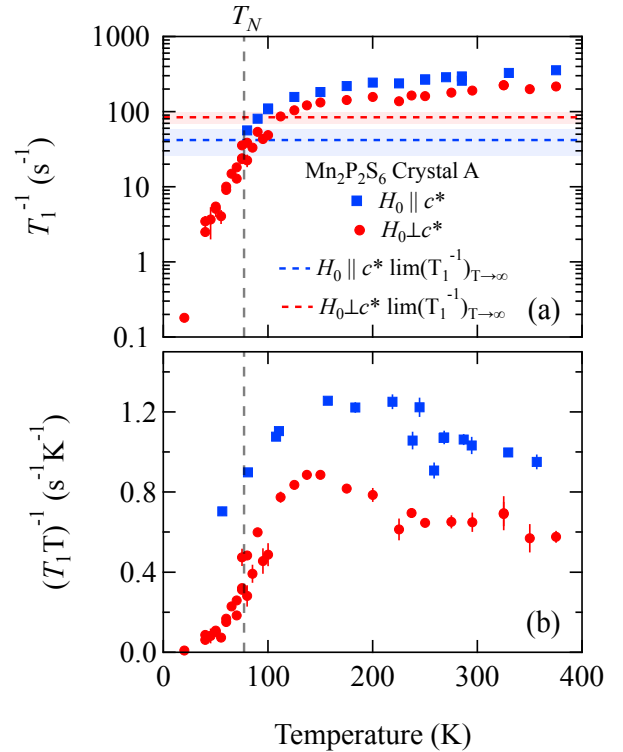


FIG. 11. (a)  $(T_1)^{-1}$  vs temperature from  $\text{Mn}_2\text{P}_2\text{S}_6$  crystal A. (b) Spin-lattice relaxation rate divided by temperature  $(T_1 T)^{-1}$  as a function of temperature for the same sample. The Néel temperature  $T_N$  is marked with a dashed vertical line.

eters from Ref. [27] and the fractional atomic positions from [37]. The calculated dipolar hyperfine coupling ten-

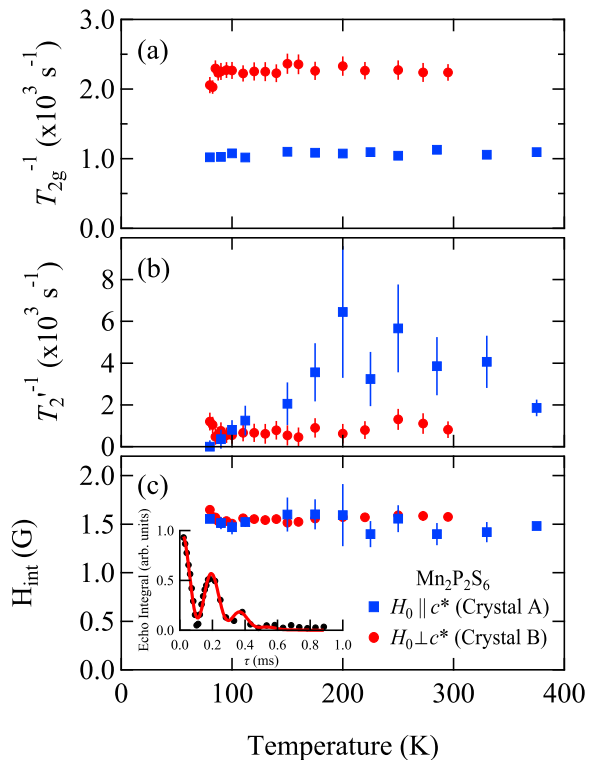


FIG. 12. Parameters  $T_{2g}^{-1}$ ,  $T_{2'}^{-1}$ , and  $H_{int}$  extracted from fits to the echo-decay curves as a function of temperature for  $\text{Mn}_2\text{P}_2\text{S}_6$ . The inset shows an example echo-decay curve (crystal B,  $H_0 \perp c^*$ ,  $T = 295$  K).

tor is given by

$$\tilde{\mathbf{A}}_{\text{dip}} = \begin{bmatrix} 0.033 & 0.000 & 0.001 \\ 0.000 & 0.035 & 0.000 \\ 0.001 & 0.000 & -0.067 \end{bmatrix}, \quad (3)$$

where all values are given in units of  $\text{T}/\mu_B$ . We have rounded the values to the third decimal place to convey that the off-diagonal components  $A_{\text{dip},xz} = A_{\text{dip},zx}$  are nonzero. We note that, to within machine precision, the other off-diagonal components are identically zero. The resulting calculated dipolar hyperfine fields—based on ordered moments of Mn with magnitude  $4.43 \pm 0.03 \mu_B$  canted  $\sim 8^\circ$  from  $c^*$  toward the  $a$  direction [27]—at the two magnetically inequivalent P sites are  $H_{\text{int,above}}^{\text{dip}} = -0.007 \text{ T } \hat{b}$ , and  $H_{\text{int,below}}^{\text{dip}} = 0.007 \text{ T } \hat{b}$ . By comparing the measured hyperfine couplings to the values from this tensor we can estimate the contribution of transferred hyperfine coupling,  $A_{\text{tr}} = A_{\text{tot}} - A_{\text{dip}}$ . These values are summarized in Table II, and show that the diagonal components of the transferred hyperfine coupling tensor are of the same order of magnitude as the dipolar hyperfine coupling.

Our measurements of the internal hyperfine field in  $\text{Mn}_2\text{P}_2\text{S}_6$  as a function of temperature are summarized in Fig. 8. We have performed a multi-peak fit and then

	$A_{\text{tot}}$ ( $\text{T}/\mu_B$ )	$A_{\text{dip}}$ ( $\text{T}/\mu_B$ )	$A_{\text{tr}}$ ( $\text{T}/\mu_B$ )
$A_{c^*}$	$-0.04 \pm 0.01$	$-0.07$	$0.05 \pm 0.01$
$A_{ab}$	$-0.02 \pm 0.01$	$0.03$	$-0.05 \pm 0.01$

TABLE II. Experimentally observed total hyperfine coupling  $A_{\text{tot}}$ , calculated dipolar coupling  $A_{\text{dip}}$ , and resultant transferred hyperfine coupling  $A_{\text{tr}} = A_{\text{tot}} - A_{\text{dip}}$ .  $A_{\text{tot}}$  are the high temperature values from Table I.  $A_{ab,\text{dip}}$  is an average of  $A_a$  and  $A_b$  from Eqn. 3.

found  $H_{int}$  by calculating the difference in frequency between a pair of magnetically split peaks of the form:

$$H_{int} = (f_2 - f_1)/(2\gamma) \quad (4)$$

where  $\gamma$  is the  $^{31}\text{P}$  nuclear gyromagnetic ratio.

We fit the measured internal field as a function of temperature to a power law of the form

$$H_{int}(T) = H_{\text{int},0} \left(1 - \frac{T}{T_N}\right)^\beta \quad (5)$$

where  $H_{\text{int},0}$  is the zero temperature internal field,  $T_N$  is the Néel temperature and  $\beta$  is the power law exponent. The least squares fit results in  $H_{\text{int},0} = 0.0087 \pm 0.0001 \text{ T}$ ,  $T_N = 76.9 \pm 0.6 \text{ K}$ , and  $\beta = 0.22 \pm 0.02$ . The value of  $\beta$  here agrees well with the two-dimensional anisotropic Heisenberg (2DAH) model value of  $\beta = 0.231$  and the previously measured value of  $\beta = 0.25 \pm 0.01$  [29, 58, 59]. The experimentally determined zero temperature internal field  $H_{\text{int},0}$  also agrees reasonably well with the calculated dipolar hyperfine field. This means that the local contribution of the static transferred hyperfine fields from the six surrounding Mn moments nearly cancel out or are individually very small.

A further magnetic state measurement that is of significant interest is the observation of  $\pm 60^\circ$  domains in both crystals of  $\text{Mn}_2\text{P}_2\text{S}_6$  that we measured, although we only show results from  $\text{Mn}_2\text{P}_2\text{S}_6$  crystal A in Fig. 7. Similar spectra were also observed in  $\text{Ni}_2\text{P}_2\text{S}_6$  crystal B from our previous work, but  $\text{Ni}_2\text{P}_2\text{S}_6$  crystal A was never measured. In this work we found that  $\text{Ni}_2\text{P}_2\text{S}_6$  crystal A only has two peaks that evolve with angle in an identical fashion as the offset spectra from  $\text{Ni}_2\text{P}_2\text{S}_6$  crystal B. This sample dependence of stacking-fault domains certainly warrants further investigation, ideally with surface-sensitive probes in a crystal with many step edges. This phenomenon may also be somewhat material dependent, as we also do not observe stacking-fault-induced spectral splitting in  $\text{Fe}_2\text{P}_2\text{S}_6$  [60].

The magnetic field dependence of the internal field also allowed us to carefully track the spin-flop transition in  $\text{Mn}_2\text{P}_2\text{S}_6$  and resulted in the discovery of a high-field spin-flop transition in  $\text{Ni}_2\text{P}_2\text{S}_6$ . As we were limited to a maximum field of 16 T, it would be very interesting to explore the evolution of this spin-flop phase in higher fields with both NMR and bulk probes, such as magnetization.

Furthermore, a recent report of the substitution dependence of the spin-flop transition in  $(\text{Ni}_{1-x}\text{Mn}_x)_2\text{P}_2\text{S}_6$  [34] motivates high-field exploration of the substitution dependence, especially for  $x < 0.5$ .

The relaxation data agree well with the literature for  $\text{Mn}_2\text{P}_2\text{S}_6$  [18], but as no field dependence of  $T_N$  was observed in  $M$  vs  $T$  at various fields up to 7 T [33], we did not investigate the field dependence of  $T_1$ . Previous measurements in several  $T_2\text{P}_2\text{X}_6$  compounds found field dependence of the magnetic transitions as well as field dependence of the spin-lattice relaxation rate. We speculate that the previously observed field dependence is related to sample quality [18, 30, 31].

We found that in  $\text{Mn}_2\text{P}_2\text{S}_6$   $(T_1T)^{-1}$  qualitatively tracks the bulk magnetic susceptibility, i.e. there is a downturn at  $T_{\text{max}}$  for both  $H_0 \parallel c^*$  and  $H_0 \perp c^*$ . This is not uncommon in local moment insulators, and may indicate that fluctuations begin to become gapped even above  $T_N$ . However, no loss of  $^{31}\text{P}$  spectral weight was observed in this temperature range, which means that, to within the experimental uncertainty, we still observe all spins in the ensemble until approximately 85 K.

In a local moment system at very high temperatures, we expect  $T_1^{-1}$  to saturate. Considering the fact that we know there to be two contributions to the total hyperfine coupling, i.e. dipole-dipole hyperfine coupling and transferred hyperfine coupling, and the fact that dipole coupling is long range, whereas transferred hyperfine coupling is short range; these two hyperfine couplings should contribute independently to relaxation of the nuclei [61–63]. We calculate the high temperature limit of  $T_1^{-1}$  for  $\text{Mn}_2\text{P}_2\text{S}_6$  based on the fluctuations of exchange-coupled moments where the total angular momentum can be approximated as  $J \approx S$  [64, 65] via:

$$\lim_{T \rightarrow \infty} \left( \frac{1}{T_1} \right) = \left( (A_{\text{dip}}^\perp)^2 + (A_{\text{tr}}^\perp)^2 \right) \sqrt{2\pi} \left( \frac{\gamma g \mu_B}{z'} \right)^2 \times \frac{z' S(S+1)}{3\omega_{ex}}, \quad (6)$$

where  $\gamma$  is the nuclear gyromagnetic ratio,  $g$  is the electron  $g$ -factor,  $A_{\text{dip}}^\perp$  and  $A_{\text{tr}}^\perp$  are the dipolar hyperfine coupling and the transferred hyperfine coupling perpendicular to the applied field, respectively,  $\mu_B$  is the Bohr magneton,  $z'$  is the number of coupled  $^{31}\text{P}$  sites,  $S$  is the spin angular momentum of the magnetic ion.  $\omega_{ex}$  is the Heisenberg exchange frequency given by,

$$\omega_{ex} = \frac{|J_{\text{ex,max}}| k_B}{\hbar} \sqrt{\frac{2zS(S+1)}{3}}, \quad (7)$$

where  $J_{\text{ex,max}}$  is the maximum exchange coupling and  $z$  is the number of exchange coupled moments [66].

The maximum of the exchange couplings is  $J_1 = -0.77 \pm 0.09$  meV, which was determined from neutron scattering experiments [58]. The calculations for  $S = 5/2$   $\text{Mn}_2\text{P}_2\text{S}_6$  yield  $\omega_{ex} = 4.9 \times 10^{12} \pm 6 \times 10^{11} \text{ s}^{-1}$ , and the calculated dipole and experimentally extracted transferred perpendicular hyperfine cou-

plings  $|A_{\text{dip}}^\perp(H_0 \parallel c^*)| = 0.03 \text{ T}/\mu_B$ ,  $|A_{\text{tr}}^\perp(H_0 \parallel c^*)| = 0.05 \pm 0.01 \text{ T}/\mu_B$ ,  $|A_{\text{dip}}^\perp(H_0 \perp c^*)| = 0.07 \text{ T}/\mu_B$ , and  $|A_{\text{tr}}^\perp(H_0 \perp c^*)| = 0.05 \pm 0.01 \text{ T}/\mu_B$ . we obtain:  $\lim_{T \rightarrow \infty} (T_1^{-1})_{\parallel} = 40 \pm 20 \text{ s}^{-1}$  for  $H_0 \parallel c^*$  and  $\lim_{T \rightarrow \infty} (T_1^{-1})_{\perp} = 80 \pm 10 \text{ s}^{-1}$  for  $H_0 \perp c^*$ . The disagreement with the experimental data (see Fig. 11) up to the highest measured temperatures may point toward the existence of nonzero off-diagonal components of the transferred hyperfine coupling tensor.

In the case of  $\text{Ni}_2\text{P}_2\text{S}_6$  we were able to perform this calculation considering only the total hyperfine couplings, because hyperfine coupling was dominated by the transferred component of the hyperfine coupling. Indeed, the high-temperature limits of  $T_1^{-1}$  for  $\text{Ni}_2\text{P}_2\text{S}_6$  based on Equation 6 are slightly larger, but well within the uncertainties in comparison to Ref. [35]:  $\lim_{T \rightarrow \infty} (T_1^{-1})_{\parallel} = 200 \pm 100 \text{ s}^{-1}$  for  $H_0 \parallel c^*$  and  $\lim_{T \rightarrow \infty} (T_1^{-1})_{\perp} = 140 \pm 80 \text{ s}^{-1}$  for  $H_0 \perp c^*$ .

Finally, we address the curious oscillatory behavior of the echo-decay curves, an example of which is shown in the inset of Fig. 12. These oscillations manifest as a result of either low energy (as compared to the scale of the linewidth) nuclear quadrupole or hyperfine interactions. In the case of  $I = 1/2$   $^{31}\text{P}$ , the nuclear quadrupole interaction does not come into play, and therefore there must be a small temperature-independent hyperfine field. This field  $H_{\text{int}}$  does not arise from static magnetism of Mn for  $T \gg T_N$ , and therefore must come from another source. The temperature-averaged experimental value of  $H_{\text{int}} = 1.53 \pm 0.02 \text{ G}$  is actually quite close to the internal field expected to be generated by homonuclear dipole-dipole coupling between the P nuclei in the P dimers, which in the case of P nuclei separated by  $R_{\text{P-P}} = 2.187(3) \text{ \AA}$  is  $H_{\text{int,Pake}} = 1.639 \pm 0.007 \text{ G}$ .

Based on the calculation of the splitting/angular dependence of the Pake doublet for  $\text{Mn}_2\text{P}_2\text{S}_6$ , we would expect a maximum splitting  $\Delta f = 5.66 \pm 0.02 \text{ kHz}$  for  $H_0 \parallel c^*$  [67]. We do observe a spectrum for this orientation with a marginally double-peaked shape, and an average temperature-independent splitting of  $8.7 \pm 0.7 \text{ kHz}$ , but the larger spectral width (average FWHM = 12.2 kHz if fit with two peaks) almost completely obscures this effect. This is different from the case of  $\text{Ni}_2\text{P}_2\text{S}_6$ , where the lines were very narrow and we could observe the doublet cleanly.

#### IV. CONCLUSIONS

In summary, we have conducted a detailed NMR study of  $\text{Mn}_2\text{P}_2\text{S}_6$ , revealing an NMR shift anomaly associated with quasi-2D magnetic correlations. We find this anomaly manifests in the vicinity of  $T_{\text{max}}$ , the maximum in the static bulk magnetic susceptibility  $\chi$ . This anomaly occurs in both  $\text{Mn}_2\text{P}_2\text{S}_6$  and  $\text{Ni}_2\text{P}_2\text{S}_6$  in spite of a factor of two difference in  $T_N$ . In the case of  $\text{Mn}_2\text{P}_2\text{S}_6$

the apparent hyperfine coupling changes sign in the low temperature regime of the paramagnetic state (approximately below  $T_{\max}$ ), possibly revealing the existence of short-range magnetic correlations, although no appreciable increase in linewidth or loss of spectral weight occur. The calculated diagonal elements of the transferred hyperfine coupling tensor are of the same order of magnitude as those of the geometrical dipole-dipole hyperfine coupling tensor.  $(T_1T)^{-1}$  qualitatively follows the peak-like behavior of  $\chi$ , indicating that NMR relaxation is also sensitive to quasi-2D correlations, which in turn points to suppression of spin fluctuations that onsets at  $T_{\max}$ .

Magnetic state NMR measurements of Mn  $_2P_2S_6$  indicate that stacking faults are not unique to the case of  $Ni_2P_2S_6$ , as the spectra split into three pairs of peaks with  $\pm 60^\circ$  rotational offset. However, upon revisiting a second crystal of  $Ni_2P_2S_6$ , we observe evidence for only one magnetic domain, and therefore demonstrate sample dependence that motivates future measurements with techniques sensitive to the existence magnetic domains and/or stacking faults. We also showed that NMR is a sensitive probe of the spin-flop transition in  $Mn_2P_2S_6$

with  $H_{sf} = 4$  T. Field-dependent spectral measurements of  $Ni_2P_2S_6$  in the magnetic state at high field reveal a similar spin-flop transition with  $H_{sf} = 14$  T. We therefore propose further high-field investigation of this compound via bulk probes, especially magnetization.

## ACKNOWLEDGMENTS

The authors would like to thank P. Fritsch, N. J. Curro, and H. Yasuoka for fruitful discussions. A.P.D. was supported by DFG Grant No. DI2538/1-1. S.A. acknowledges financial support of (DFG) through Grant No AS 523/4-1. S.S. acknowledges financial support from the graduate academy GRK-1621 of the DFG (Project No. 129760637). A.B. and F.B. acknowledge financial support of Tunisian Ministry of Higher Education and Scientific Research. B.B. S.A. & Y.S. acknowledge financial support of BMBF through UKRATOP (BMBF), under reference 01DK18002.

- 
- [1] We denote the chemical formula using doubled notation due to the presence of the particular  $(P_2Ch_6)^{4-}$  unit, which forms a structural motif in this class of compounds [5, 68, 69].
- [2] X. Li, T. Cao, Q. Niu, J. Shi, and J. Feng, Coupling the valley degree of freedom to antiferromagnetic order, *Proceedings of the National Academy of Sciences* **110**, 3738 (2013).
- [3] H. Li, S. Ruan, and Y.-J. Zeng, Intrinsic Van Der Waals Magnetic Materials from Bulk to the 2D Limit: New Frontiers of Spintronics, *Advanced Materials* **31**, 1900065 (2019).
- [4] K. S. Burch, D. Mandrus, and J.-G. Park, Magnetism in two-dimensional van der Waals materials, *Nature* **563**, 47 (2018).
- [5] R. Brec, Review on Structural and Chemical Properties of Transition Metal Phosphorus Trisulfides  $MPS_3$ , in *Intercalation in Layered Materials* (Springer US, 1986) pp. 93–124.
- [6] V. Grasso, S. Santangelo, and M. Piacentini, Optical absorption spectra of some transition metal thiophosphates, *Solid State Ionics* **20**, 9 (1986).
- [7] P. A. Joy and S. Vasudevan, Magnetism in the layered transition-metal thiophosphates  $MPS_3$  ( $M = Mn, Fe,$  and  $Ni$ ), *Physical Review B* **46**, 5425 (1992).
- [8] V. Grasso, F. Neri, S. Patanè, L. Silipigni, and M. Piacentini, Conduction processes in the layered semiconductor compound  $FePS_3$ , *Physical Review B* **42**, 1690 (1990).
- [9] R. Brec, D. M. Schleich, G. Ouvrard, A. Louisy, and J. Rouxel, Physical properties of lithium intercalation compounds of the layered transition-metal chalcogenophosphites, *Inorganic Chemistry* **18**, 1814 (1979).
- [10] A. Simon, J. Ravez, V. Maisonneuve, C. Payen, and V. B. Cajipe, Paraelectric-Ferroelectric Transition in the Lamellar Thiophosphate  $CuInP_2S_6$ , *Chemistry of Materials* **6**, 1575 (1994).
- [11] S. Yitzchaik, S. D. Bella, P. M. Lundquist, G. K. Wong, and T. J. Marks, Anomalous Second-Order Nonlinear Optical Response of In-Plane Poled Glassy Polymers. Spectroscopic and Theoretical Support for the Importance of Charged Chromophore Aggregates, *Journal of the American Chemical Society* **119**, 2995 (1997).
- [12] P. G. Lacroix, R. Clement, K. Nakatani, J. Zyss, and I. Ledoux, Stilbazolium- $MPS_3$  Nanocomposites with Large Second-Order Optical Nonlinearity and Permanent Magnetization, *Science* **263**, 658 (1994).
- [13] I. Lagadic, P. G. Lacroix, and R. Clément, Layered  $MPS_3$  ( $M = Mn, Cd$ ) Thin Films as Host Matrixes for Nonlinear Optical Material Processing, *Chemistry of Materials* **9**, 2004 (1997).
- [14] P. A. Joy and S. Vasudevan, The intercalation reaction of pyridine with manganese thiophosphate,  $MnPS_3$ , *Journal of the American Chemical Society* **114**, 7792 (1992).
- [15] M. C. Friedel, Sur une nouvelle série de sulfophosphures, les thiohypophosphates, *C. R. Acad. Sci.* **119**, 260 (1894).
- [16] R. Nitsche and P. Wild, Crystal growth of metal-phosphorus-sulfur compounds by vapor transport, *Materials Research Bulletin* **5**, 419 (1970).
- [17] B. E. Taylor, J. Steger, and A. Wold, Preparation and properties of some transition metal phosphorus trisulfide compounds, *Journal of Solid State Chemistry* **7**, 461 (1973).
- [18] C. Berthier, Y. Chabre, and M. Minier, NMR investigation of the layered transition metal phosphorus trichalcogenides and the intercalation compounds  $Li_xNiPS_3$ , *Solid State Communications* **28**, 327 (1978).
- [19] X. Wang, J. Cao, Z. Lu, A. Cohen, H. Kitadai, T. Li, Q. Tan, M. Wilson, C. H. Lui, D. Smirnov, S. Sharifzadeh, and X. Ling, Spin-induced linear polarization of

- photoluminescence in antiferromagnetic van der Waals crystals, *Nature Materials* **20**, 964 (2021).
- [20] K. Kim, S. Y. Lim, J.-U. Lee, S. Lee, T. Y. Kim, K. Park, G. S. Jeon, C.-H. Park, J.-G. Park, and H. Cheong, Suppression of magnetic ordering in XXZ-type antiferromagnetic monolayer NiPS<sub>3</sub>, *Nature Communications* **10**, 345 (2019).
- [21] S. Y. Kim, T. Y. Kim, L. J. Sandilands, S. Sinn, M.-C. Lee, J. Son, S. Lee, K.-Y. Choi, W. Kim, B.-G. Park, C. Jeon, H.-D. Kim, C.-H. Park, J.-G. Park, S. Moon, and T. Noh, Charge-Spin Correlation in van der Waals Antiferromagnet NiPS<sub>3</sub>, *Physical Review Letters* **120**, 136402 (2018).
- [22] Y. Wang, Z. Zhou, T. Wen, Y. Zhou, N. Li, F. Han, Y. Xiao, P. Chow, J. Sun, M. Pravica, A. L. Cornelius, W. Yang, and Y. Zhao, Pressure-Driven Cooperative Spin-Crossover, Large-Volume Collapse, and Semiconductor-to-Metal Transition in Manganese(II) Honeycomb Lattices, *Journal of the American Chemical Society* **138**, 15751 (2016).
- [23] X. Ma, Y. Wang, Y. Yin, B. Yue, J. Dai, J. Cheng, J. Ji, F. Jin, F. Hong, J.-T. Wang, Q. Zhang, and X. Yu, Dimensional crossover tuned by pressure in layered magnetic NiPS<sub>3</sub>, *Science China Physics Mechanics & Astronomy* **64**, 297011 (2021).
- [24] D. Lançon, H. C. Walker, E. Ressouche, B. Oulad-diaf, K. C. Rule, G. J. McIntyre, T. J. Hicks, H. M. Rønnow, and A. R. Wildes, Magnetic structure and magnon dynamics of the quasi-two-dimensional antiferromagnet FePS<sub>3</sub>, *Physical Review B* **94**, 214407 (2016).
- [25] H.-S. Kim, K. Haule, and D. Vanderbilt, Mott Metal-Insulator Transitions in Pressurized Layered Trichalcogenides, *Physical Review Letters* **123**, 236401 (2019).
- [26] V. Grasso and L. Silipigni, Low-dimensional materials: The MPX<sub>3</sub> family, physical features and potential future applications, *La Rivista del Nuovo Cimento* **25**, 1 (2002).
- [27] E. Ressouche, M. Loire, V. Simonet, R. Ballou, A. Stunault, and A. Wildes, Magnetoelectric MnPS<sub>3</sub> as a candidate for ferrotoroidicity, *Physical Review B* **82**, 100408 (2010).
- [28] A. R. Wildes, H. M. Rønnow, B. Roessli, M. J. Harris, and K. W. Godfrey, Anisotropy and the critical behaviour of the quasi-2D antiferromagnet, MnPS<sub>3</sub>, *Journal of Magnetism and Magnetic Materials* **310**, 1221 (2007).
- [29] A. R. Wildes, H. M. Rønnow, B. Roessli, M. J. Harris, and K. W. Godfrey, Static and dynamic critical properties of the quasi-two-dimensional antiferromagnet MnPS<sub>3</sub>, *Physical Review B* **74**, 094422 (2006).
- [30] J. Ziolo, S. Torre, A. Rigamonti, and F. Borsa, <sup>31</sup>P NMR relaxation study of spin dynamics in layered transition-metal compounds MPX<sub>3</sub>, *Journal of Applied Physics* **63**, 3095 (1988).
- [31] S. Torre and J. Ziolo, Spin dynamics and magnetic properties of two-dimensional systems MPX<sub>3</sub> from <sup>31</sup>P NMR and relaxation, *Physical Review B* **39**, 8915 (1989).
- [32] S. Selter, Y. Shemerliuk, M.-I. Sturza, A. U. B. Wolter, B. Büchner, and S. Aswartham, Crystal growth and anisotropic magnetic properties of quasi-two-dimensional (Fe<sub>1-x</sub>Ni<sub>x</sub>)<sub>2</sub>P<sub>2</sub>S<sub>6</sub>, *Physical Review Materials* **5**, 073401 (2021).
- [33] Y. Shemerliuk, Y. Zhou, Z. Yang, G. Cao, A. U. B. Wolter, B. Büchner, and S. Aswartham, Tuning Magnetic and Transport Properties in Quasi-2D (Mn<sub>1-x</sub>Ni<sub>x</sub>)<sub>2</sub>P<sub>2</sub>S<sub>6</sub> Single Crystals, *Electronic Materials* **2**, 284 (2021).
- [34] R. Basnet, A. Wegner, K. Pandey, S. Storment, and J. Hu, Highly sensitive spin-flop transition in antiferromagnetic van der Waals material MPS<sub>3</sub> (*M* = Ni and Mn), *Physical Review Materials* **5**, 064413 (2021).
- [35] A. P. Dioguardi, S. Selter, U. Peeck, S. Aswartham, M.-I. Sturza, R. Murugesan, M. S. Eldeeb, L. Hozoi, B. Büchner, and H.-J. Grafe, Quasi-two-dimensional magnetic correlations in Ni<sub>2</sub>P<sub>2</sub>S<sub>6</sub> probed by <sup>31</sup>P NMR, *Physical Review B* **102**, 064429 (2020).
- [36] T. Masubuchi, H. Hoya, T. Watanabe, Y. Takahashi, S. Ban, N. Ohkubo, K. Takase, and Y. Takano, Phase diagram, magnetic properties and specific heat of Mn<sub>1-x</sub>Fe<sub>x</sub>PS<sub>3</sub>, *Journal of Alloys and Compounds* **460**, 668 (2008).
- [37] G. Ouvrard, R. Brec, and J. Rouxel, Structural determination of some MPS<sub>3</sub> layered phases (*M* = Mn, Fe, Co, Ni and Cd), *Materials Research Bulletin* **20**, 1181 (1985).
- [38] K. Momma and F. Izumi, VESTA 3 for three-dimensional visualization of crystal, volumetric and morphology data, *Journal of Applied Crystallography* **44**, 1272 (2011).
- [39] R. K. Harris, E. D. Becker, S. M. C. de Menezes, R. Goodfellow, and P. Granger, NMR nomenclature. Nuclear spin properties and conventions for chemical shifts(IUPAC Recommendations 2001), *Pure and Applied Chemistry* **73**, 1795 (2001).
- [40] J. A. Osborn, Demagnetizing factors of the general ellipsoid, *Physical Review* **67**, 351 (1945).
- [41] A. M. Clogston, V. Jaccarino, and Y. Yafet, Interpretation of Knight Shifts and Susceptibilities of Transition Metals: Platinum, *Physical Review* **134**, A650 (1964).
- [42] K. Okuda, K. Kurosawa, S. Saito, M. Honda, Z. Yu, and M. Date, Magnetic Properties of Layered Compound MnPS<sub>3</sub>, *Journal of the Physical Society of Japan* **55**, 4456 (1986).
- [43] D. J. Goossens, A. R. Wildes, C. Ritter, and T. J. Hicks, Ordering and the nature of the spin flop phase transition in MnPS<sub>3</sub>, *Journal of Physics: Condensed Matter* **12**, 1845 (2000).
- [44] A. R. Wildes, V. Simonet, E. Ressouche, G. J. McIntyre, M. Avdeev, E. Suard, S. A. J. Kimber, D. Lançon, G. Pepe, B. Moubaraki, and T. J. Hicks, Magnetic structure of the quasi-two-dimensional antiferromagnet NiPS<sub>3</sub>, *Physical Review B* **92**, 224408 (2015).
- [45] S. Strässle, B. Graneli, M. Mali, J. Roos, and H. Keller, Absence of Orbital Currents in Superconducting YBa<sub>2</sub>Cu<sub>4</sub>O<sub>8</sub> Using a Zeeman-Perturbed Nuclear-Quadrupole-Resonance Technique, *Physical Review Letters* **106**, 097003 (2011).
- [46] K. R. Shirer, A. C. Shockley, A. P. Dioguardi, J. Crocker, C. H. Lin, N. apRoberts Warren, D. M. Nisson, P. Klavins, J. C. Cooley, Y. f. Yang, and N. J. Curro, Long range order and two-fluid behavior in heavy electron materials, *Proceedings of the National Academy of Sciences* **109**, E3067 (2012).
- [47] N. J. Curro, B.-L. Young, J. Schmalian, and D. Pines, Scaling in the emergent behavior of heavy-electron materials, *Physical Review B* **70**, 235117 (2004).
- [48] G. Stemmman, C. Pépin, and M. Lavagna, Spin gap and magnetic excitations in the cuprate superconductors, *Physical Review B* **50**, 4075 (1994).
- [49] J. Thoma, S. Tewari, J. Ruvalds, and C. T. Rieck, Susceptibility and Knight-shift anomalies in cuprate superconductors, *Physical Review B* **51**, 15393 (1995).

- [50] A. S. Moskvin, Field-induced staggered magnetization and  $^{17}\text{O}$  Knight shift anomaly in  $\text{La}_2\text{CuO}_4$ , *Physical Review B* **75**, 054505 (2007).
- [51] Y. P. Wu, D. Zhao, A. F. Wang, N. Z. Wang, Z. J. Xiang, X. G. Luo, T. Wu, and X. H. Chen, Emergent Kondo Lattice Behavior in Iron-Based Superconductors  $\text{AFe}_2\text{As}_2$  ( $A = \text{K}, \text{Rb}, \text{Cs}$ ), *Physical Review Letters* **116**, 147001 (2016).
- [52] N. J. Curro, Nuclear magnetic resonance in the heavy fermion superconductors, *Reports on Progress in Physics* **72**, 026502 (2009).
- [53] V. Grasso, F. Neri, P. Perillo, L. Silipigni, and M. Piacentini, Optical-absorption spectra of crystal-field transitions in  $\text{MnPS}_3$  at low temperatures, *Physical Review B* **44**, 11060 (1991).
- [54] J. J. van der Klink and H. B. Brom, Relation between susceptibility and Knight shift in  $\text{La}_2\text{NiO}_{4.17}$  and  $\text{K}_2\text{NiF}_4$  by  $^{61}\text{Ni}$  NMR, *Physical Review B* **81**, 094419 (2010).
- [55] R. Sarkar, Z. Mei, A. Ruiz, G. Lopez, H.-H. Klauss, J. G. Analytis, I. Kimchi, and N. J. Curro, Impact of disorder on dynamics and ordering in the honeycomb-lattice iridate  $\text{Na}_2\text{IrO}_3$ , *Physical Review B* **101**, 081101 (2020).
- [56] A. Wiedenmann, J. Rossat-Mignod, A. Louisy, R. Brec, and J. Rouxel, Neutron diffraction study of the layered compounds  $\text{MnPS}_3$  and  $\text{FePS}_3$ , *Solid State Communications* **40**, 1067 (1981).
- [57] H.-J. Grafe, S. Nishimoto, M. Iakovleva, E. Vavilova, L. Spillecke, A. Alfonsov, M.-I. Sturza, S. Wurmehl, H. Nojiri, H. Rosner, J. Richter, U. K. Rößler, S.-L. Drechsler, V. Kataev, and B. Büchner, Signatures of a magnetic field-induced unconventional nematic liquid in the frustrated and anisotropic spin-chain cuprate  $\text{LiCuSbO}_4$ , *Scientific Reports* **7**, 6720 (2017).
- [58] A. R. Wildes, B. Roessli, B. Lebech, and K. W. Godfrey, Spin waves and the critical behaviour of the magnetization in  $\text{MnPS}_3$ , *Journal of Physics: Condensed Matter* **10**, 6417 (1998).
- [59] S. T. Bramwell and P. C. W. Holdsworth, Magnetization and universal sub-critical behaviour in two-dimensional XY magnets, *Journal of Physics: Condensed Matter* **5**, L53 (1993).
- [60] U. Peeck, *NMR Study on  $\text{Fe}_2\text{P}_2\text{S}_6$* , Master's thesis, Technische Universität Dresden (2021).
- [61] H.-J. Grafe, G. Lang, F. Hammerath, D. Paar, K. Manthey, K. Koch, H. Rosner, N. J. Curro, G. Behr, J. Werner, N. Leps, R. Klingeler, H.-H. Klauss, F. J. Litterst, and B. Büchner, Electronic properties of  $\text{LaO}_{1-x}\text{F}_x\text{FeAs}$  in the normal state probed by NMR/NQR, *New Journal of Physics* **11**, 035002 (2009).
- [62] N. J. Curro and L. Morales, Nuclear Magnetic Resonance Studies of  $\delta$ -Stabilized Plutonium, *MRS Proceedings* **802**, 53 (2003).
- [63] T. Imai, C. P. Slichter, K. Yoshimura, and K. Kosuge, Low frequency spin dynamics in undoped and Sr-doped  $\text{La}_2\text{CuO}_4$ , *Physical Review Letters* **70**, 1002 (1993).
- [64] T. Moriya, Nuclear Magnetic Relaxation in Antiferromagnetics, *Progress of Theoretical Physics* **16**, 23 (1956).
- [65] T. Moriya, Nuclear Magnetic Relaxation in Antiferromagnetics, II, *Progress of Theoretical Physics* **16**, 641 (1956).
- [66] R. Nath, Y. Furukawa, F. Borsa, E. E. Kaul, M. Baenitz, C. Geibel, and D. C. Johnston, Single-crystal  $^{31}\text{P}$  NMR studies of the frustrated square-lattice compound  $\text{Pb}_2(\text{VO})(\text{PO}_4)_2$ , *Physical Review B* **80**, 214430 (2009).
- [67] G. E. Pake, Nuclear Resonance Absorption in Hydrated Crystals: Fine Structure of the Proton Line, *The Journal of Chemical Physics* **16**, 327 (1948).
- [68] M. Piacentini, V. Grasso, S. Santangelo, M. Fanfoni, S. Modesti, and A. Savoia, Soft X-ray absorption of  $\text{FePS}_3$  and  $\text{NiPS}_3$ , *Solid State Communications* **51**, 467 (1984).
- [69] G. Ouvrard, E. Sandre, and R. Brec, Synthesis and crystal structure of a new layered phase: The chromium hexatellurosilicate  $\text{Cr}_2\text{Si}_2\text{Te}_6$ , *Journal of Solid State Chemistry* **73**, 27 (1988).